An Automatic Image Registration for Applications in Remote Sensing

Youcef Bentoutou, Nasreddine Taleb, Kidiyo Kpalma, and Joseph Ronsin

***Abstract*—This paper deals with a major problem encountered in the area of remote sensing consisting of the registration of multitemporal and/or multisensor images. In general, such images have different gray-level characteristics, and simple techniques such as those based on correlation cannot be applied directly. In this work, a new automatic satellite image registration approach is proposed. This technique exploits the invariant relations between regions of a reference and a sensed image, respectively. It involves an edge-based selection of the most distinctive control points (CPs) in the reference image. The search for the corresponding CPs in the sensed image is based on local similarity detection by means of template matching according to a combined invariants-based similarity measure. The final warping of the images according to the selected CPs is performed by using the thin-plate spline interpolation. The procedure is fully automatic and computationally efficient. The proposed algorithm for this technique has been successfully applied to register multitemporal SPOT and synthetic aperture radar images from urban and agricultural areas. The experimental results demonstrate the robustness, efficiency and accuracy of the algorithm.**

***Index Terms*—Feature extraction, image matching, image registration, remote sensing.**

I. Introduction

IMAGE registration is a classical problem encountered in many image processing applications where it is necessary to perform joint analysis of two or more images of the same scene acquired by different sensors, or images taken by the same sensor but at different times. Examples of these applications include change detection using multiple images acquired at different times [1], cartography and photogrammetry using imagery with overlapping coverage, and fusion of image data from multiple sensor types (e.g., low-resolution multispectral image and high-resolution panchromatic one) [2].

Given two images, I_1 (defined as a reference image) and I_2 (defined as a sensed image) to match the reference image, the goal of image registration is to rectify the sensed image into the coordinate system of the reference image and to make corresponding coordinate points in the two images fit the same geographical location. These unregistered images may have relative translation, rotation, scale between them; they may be degraded by a linear shift-invariant blur and corrupted by an additive random noise.

In remote sensing applications, one generally uses manual registration, which is not feasible in cases where a large number of images need to be registered. Thus, there is a need for automated techniques that require little or no operator supervision. The automatic image registration addresses the problems associated with manual image registration. However, there still exist a number of scenarios where automatic image registration is not well developed for multitemporal and/or multisensor image registration. The traditional procedure for manually registering a pair of satellite images requires the manual selection of control points in each image. These points are used to determine the parameters of a transformation function, which is subsequently used to register the sensed image to the reference one, by warping one of the images with respect to the other using any interpolation function. Automation of this procedure requires the replacement of the manual control point selection with automatic algorithms for locating corresponding points in both images [3].

The registration process is usually carried out in four steps. The first step consists of selection of features on the images. Next, each feature in one image is compared with potential corresponding features in the other one. A pair of points with similar attributes is accepted as matches and they are called control poins (CPs). Finally the parameters of the best transformation which models the deformation between both images are estimated using the CPs obtained in the previous step.

A. Current Approaches

An image registration algorithm suitable for remote sensing use has to meet several criteria.

1) It should be accurate.
2) It should be reliable. Hence, it should be able to handle all the occurring displacements and gray-level variations between the two images.
3) Finally, after fulfilling the above two conditions, the registration should be as fast as possible and ideally fully automatic.

Several image registration techniques have been developed [3], [4]. Unfortunately, none of these techniques has been shown to satisfy all of the above criteria. A review of recent as well as classic image registration methods has been surveyed in [4]. Current image registration techniques are generally divided into two broad categories: area-based and feature-based techniques.

Image registration with the most developed class of area-based techniques promises to be fully automatic [5], [6]. It works correctly when the input images are very similar

Manuscript received February 6, 2004; revised January 10, 2005.

Y. Bentoutou is with the National Center of Space Techniques (CNTS), Arzew, 31200, Algeria (e-mail: bentyou@cnts.dz).

N. Taleb is with the Department of Electronics, University of Sidi-Bel-Abbes, 22000, Algeria (e-mail: ne_taleb@univ-sba.dz).

K. Kpalma and J. Ronsin are with the Department of Electronics and Industrial Informatics, Institut National des Sciences Appliquees de Rennes, 35043 Rennes Cedex, France (e-mail: kidiyo.kpalma@insa-rennes.fr; ronsin@insa-rennes.fr).

Digital Object Identifier 10.1109/TGRS.2005.853187

but frequently leads to misregistration when dissimilarities are present in the images. In this case, these methods do not satisfy the second constraint. For most of these techniques, some function is defined that quantifies the similarity between the image pairs. The parameter set for which this function is optimal is then taken as the registration transform. The search for this optimum is time consuming since it often requires many function evaluations. Hence, these area-based techniques tend to be somewhat slow. Commonly used area-based similarity functions include correlation, the mean square difference of the image intensity values, and mutual information (MI). The normalized cross-correlation measure is one of the most common similarity functions used in registration. The centers of the matched windows are used as CPs to solve for the transformation parameters between the two images. The correlation measures perform well when the two images to be matched are similar but they become unreliable when the gray-level characteristics of the images are quite different. Mutual information is one of the few intensity-based measures that are well suited to registration of multimodal images [7]–[9]. Unlike measures based on correlation of gray values or differences of gray values, mutual information does not assume a linear relationship between the gray values in the images. The registration algorithm proposed by Thevenaz and Unser in [9] is based on a combination of mutual information together with a multiresolution gradient search. They developed a new optimizer, which takes benefit of the Marquardt–Levenberg strategy, for solving the problem of intermodal image registration, and which works in conjunction with a high-quality multiresolution representation of the image based on cubic splines. Mutual information (MI) has been studied for the registration of remote sensing imagery [10]–[13], and it has been found to be especially robust for multisensor image registration. The transformation which maximizes MI has been determined using exhaustive search [10]–[12], but this has been found to be inefficient and computationally expensive [13]. A multiresolution registration technique proposed recently in [13] combined a powerful search strategy based on a stochastic gradient with two similarity measures, correlation and mutual information, together with a wavelet-based multiresolution pyramid. In this recent work, mutual information has been shown to be better suited for subpixel registration as it produces consistently sharper optimum peaks than correlation [13]. This approach has been applied to registering images with rotational and/or translational differences rather than the natural remotely sensed images with general affine distortion. Affine distortion appears in remote sensing very often; it describes for example the image skew caused by the Earth's rotation [14].

In contrast to the area-based methods, the feature-based ones do not work directly with image intensity values [5], [14]–[22]. Feature-based methods, which extract and match salient features from two images, have been shown to be more suitable for situations when illumination changes are expected or multisensor analysis is performed [5], [20]. There are two critical procedures generally involved in the feature-based techniques: feature detection and feature matching [21]. The first procedure consists of detecting manually or, preferably, automatically a set of distinctive objects such as closed-boundary regions, edges, contours, line intersections, and corners. A variety of image segmentation and edge detection techniques have been used for feature extraction [4]. For further processing, these features can be represented by their point representatives (centers of gravity of closed boundaries [14], [16], [21] and distinctive points [5]), which are called control points in the literature [4]. Feature matching is one of the most important tasks in automated image registration. In this procedure, the correspondence between the features detected in the sensed image and those detected in the reference image is established. Various feature descriptors and similarity measures, such as binary correlation, chain-code correlation, distance of invariant moments, structural matching, Chamfer matching, dynamic programming, and relaxation algorithms, are used for that purpose [4]. A drawback of the existing feature-based techniques lies in the difficulty of recognizing matched features in the images.

Satellite image registration with the most recently developed model incorporating multiple feature extraction algorithms promises to be accurate [21], [22]. However, in both images identical CPs have to be detected manually, which is time-consuming for an operator. Moreover, some extra time has to be added for multiple feature extraction. Consequently, multiple feature extraction and the necessary human supervision make the registration slow and far from fully automatic.

B. Aim of the Paper

The purpose of this paper is to demonstrate that using a gradient-based control point selection mechanism and using the combined invariants-based similarity measure for CP displacement computation, lead to a registration algorithm that satisfies all the constraints mentioned at the beginning of this section and thus can efficiently improve the quality of the registered images. The proposed registration method is performed by applying the elastic thin-plate spline (TPS) interpolating registration on sets of CP pairs [23]. This interpolation model plays an essential role to reach subpixel accuracy. The designed algorithm has the capability to register images both globally and locally. This algorithm, introducing local processing on areas of interest based on control pixels, is fast compared to all traditional algorithms where entire images are searched, and as will be seen, demonstrates the capability to really register satellite images with accuracy. The proposed algorithm, using the TPS interpolation, has been designed to be applied on satellite images as well as on low-altitude aerial pictures of rough terrain.

The rest of the paper is organized as follows. The proposed registration approach is described in detail in Section II. Results of experiments on real data sets are reported in Section III. Finally, the related conclusions are given in Section IV.

II. Registration Approach

In this paper, the registration process is carried out in the following three steps.

1) The first step consists of selecting automatically a set of control points $P = \{p_i\}$ from the reference image.
2) In the second step, the displacements of the selected control points $p_i \in P$ are computed by means of template matching using the combined invariants-based similarity

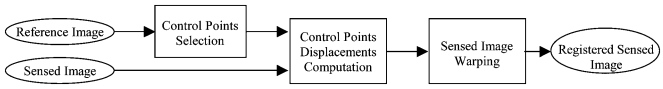

Fig. 1. Summary of the proposed automatic image registration method.

measure. The corresponding coordinates of the selected CPs in the sensed image constitute the set of CPs $Q = \{q_i\}$ in this image.

3) Last, the parameters of the best transformation which models the deformation between the images are estimated using the two sets of corresponding control points (P and Q). Then the final correction is performed according to this transformation by warping one of the images with respect to the other one using the TPS interpolation function and the estimated parameters [23].

This proposed registration approach is summarized in Fig. 1.

A. Control Points Selection

In order to obtain the correspondence between two images, area-based techniques would explicitly compute the correspondence for every pixel. However, this is computationally very expensive and will not lead to practically acceptable algorithms. In order to reduce the computation time to an acceptable level, a frequently used approach is to consider only a limited set of so-called interest points, where the image information is supposed to be the most important [24]. It has to be noted that in the particular case of satellite images, misalignment between reference and sensed images is more visible at the image edges than at the homogeneous regions. Therefore one easy way to speed up the algorithm and to reduce the computation time is to process some few pixels belonging to regions that contain significant gray-level variations (referred to as the control points), instead of processing all image edges. Obviously, the less complex the image, the faster the algorithm [19].

1) Edge Detection: The first step in the selection of the CPs consists of finding image edges. The location of edges can easily be computed by detecting local maxima of the gray-level gradient magnitude. Since edges are scale dependent image features, they can only be detected properly using derivatives calculated at the proper scale. The commonly used edge detection filter for this purpose is Gaussian derivative that allows finer tuning to detect the required edge scale [25]. It should be noted that it is necessary to indicate which edges are important for extracting adequate CPs. This is done by thresholding the gradient magnitude image at a value T_G, resulting in a binary image consisting of connected regions that are of interest. The value of the threshold T_G is assigned as the average gradient magnitude [26].

2) Control Points Detection: To select CPs in the reference image, the second step consists of detecting interest points that have stronger strength than most of other pixels in this image. The strength is basically measured by the change in pixel values along two-dimensional directions. Schmid *et al.* [26] evaluated and compared different interest point detectors and concluded that the best results are provided by the Harris detector [27]. In this paper, an improved version of the Harris corner detector [26] is used to detect points of interest in the reference image. This detector uses only first-order derivatives and is well known as one of the most stable and robust corner detectors in image processing. The basic idea is to use the autocorrelation function in order to determine locations where the signal changes in two directions. A matrix related to the autocorrelation function that takes into account the first derivatives of the signal on a window is computed. The eigenvectors of this matrix are the principal curvatures of the autocorrelation function. Two significant values indicate the presence of an interest point. The Harris detector is defined as the positive local extreme of the following operator:

$$S = \det(C) - \alpha \operatorname{trace}^2(C) \tag{1}$$

where scalar α is equal to 0.04 as suggested in [27] and the matrix C, which is related to the autocorrelation function, is given by

$$C = \begin{bmatrix} \left(\frac{\partial I}{\partial x}\right)^2 & \left(\frac{\partial I}{\partial x}\right) \cdot \left(\frac{\partial I}{\partial y}\right) \\ \left(\frac{\partial I}{\partial x}\right) \cdot \left(\frac{\partial I}{\partial y}\right) & \left(\frac{\partial I}{\partial y}\right)^2 \end{bmatrix} \tag{2}$$

where I is the gray-level intensity image. To implement this detector, the standard default parameter values recommended by the authors, are used in this work. The Harris detector [27] computes the derivatives of the matrix C by convolution with the mask $[-2\ -1\ 0\ 1\ 2]$. A Gaussian with standard deviation $(\sigma = 2)$ is used to weight the derivatives. In an improved version of Harris [26], the derivatives of the matrix C are computed more precisely by replacing the $[-2\ -1\ 0\ 1\ 2]$ mask with derivatives of a Gaussian $(\sigma = 1)$. A corner is detected when the two eigenvalues of C are large since this indicates grayscale variations in both the x and y directions. To avoid the extraction of the eigenvalues of the matrix C, the strength of interest points is measured by the operator S of (1). Nonmaximum suppression using a 3×3 mask is then applied to strength and a threshold T is used to select interest points (referred to as the control points). The threshold is set to 1% of the maximum observed interest point strength [26]. To spread out the detected CPs (corners), a user-defined distance is incorporated. Finally, the algorithm will automatically produce the extracted CPs that satisfy the above criteria and maximize the strength function. The number of these CPs is user-defined and incorporated prior to running the detector.

In this implementation, the CPs are detected in the reference image by applying the improved version of the Harris corner detector at regions where the gradient magnitude is high. This has the following two advantages.

1) The time complexity is reduced by excluding pixels with low values of gradient magnitude from computation.
2) Since the neighborhoods of those interest points are known to be structured, the reliability of the matching step will be high.

3) Control Points Selection Algorithm: The following is a summary of the different steps to be followed in the selection of CPs.

Step 1) Compute the gradient of the reference image. It is based on an edge detection filtering with the application of Gaussian derivative $(\sigma = 1)$ [25].

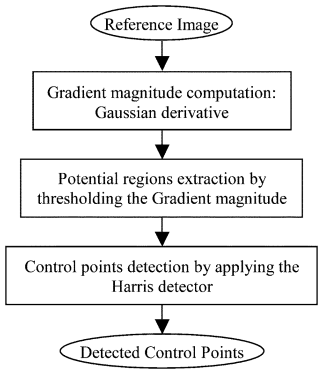

Fig. 2. Gradient-based CP selection mechanism.

Step 2) Extract potential regions by means of thresholding the gradient magnitude image at level T_G (T_G = average gradient magnitude) and setting their pixels p to "1".

Step 3) For each pixel p in the reference image compute the strength S according to (1).

Step 4) Apply nonmaximum suppression to the strength by using a 3×3 mask.

Step 5) Extract strong corners by means of thresholding the strength at level T.

Step 6) Retain the first n corners of large strength as control points if their distance is higher than the minimum allowed distance $d_{\min}$.

Fig. 2 shows a block diagram of this selection algorithm. An example of CPs selection based on this approach is shown in Fig. 3.

B. Control Points Displacements Computation

After the CPs are detected from the reference image in the previous section, a correspondence mechanism between image regions around these points must be established to match these two images. This correspondence mechanism is called template matching. Template matching techniques are based on the assumption that the displacement d of every CP in an image $I_R(x,y)$ can be approximated by taking a small window W_d around the point and finding the corresponding window in the unregistered image $I_S(x,y)$, according to a certain similarity measure.

The most important aspect of template matching is the similarity measure that is used to determine the degree of resemblance of windows in two images. Several measures have been devised and applied to register images, including correlation, normalized cross-correlation, statistical correlation, matched filters, phase-correlation, sum of absolute differences, root mean square, and masked correlation [3], [4]. However, most of these similarity measures do not satisfy the three constraints that have been emphasized in the introduction of this paper. They are sensitive to mean gray-level offsets and local geometric distortion. In addition to these fundamental problems, there are other factors that may complicate the process of finding the optimal correspondence between images. These are due to imperfections of the imaging system, such as limited spatial resolution, gray-level quantization, blur, and noise.

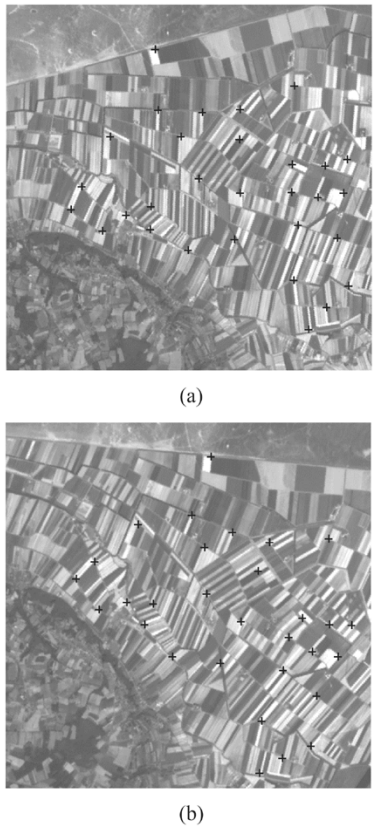

(a)

(b)

Fig. 3. Control points detection on two SPOT panchromatic images of the region of Mont Saint-Michel in Normandie (France), acquired at different dates. (a) The set of selected CPs (black crosses), with the reference image superimposed. These interest points are detected by applying the improved version of the Harris detector at potential regions where the gradient magnitude is high. The number n of CPs is 30 and the minimum allowed distance $d_{\min}$ between the points is 30 pixels. (b) The corresponding set of the selected CPs (black crosses), with the sensed image superimposed. These corresponding points in the sensed image are detected by means of template matching according to the invariant approach.

1) Combined Invariants-Based Similarity Measure: Since the images may have translational, rotational, and scaling differences, the similarity measures should be invariant with respect to translation, rotation, and scaling. Measures that are very robust against these phenomena are those of the moment-based combined invariants (i.e., invariants with respect to degradations composed from symmetric blur and other geometric or gray-level transforms) [28]. Detailed definitions of these combined invariants can be found in literature (see [28]).

The moment of a window W_d inside an image $I(i,j)$ is given by

$$m_{pq} = \sum_{(i,j)\in W_d} i^p j^q I(i,j) \tag{3}$$

where $(p+q)$ is the order of moment.

The central moment of W_d is defined as

$$\mu_{pq} = \sum_{(i,j)\in W_d} (i-x_t)^p (j-y_t)^q \, I(i,j) \tag{4}$$

where $x_t = (m_{10}/m_{00})$ and $y_t = (m_{01}/m_{00})$ are the coordinates of the center of gravity of W_d. Central moments are translational invariants. Under a scale change $i' = \alpha i$ and $j' = \alpha j$, the normalized central moments are defined as $\nu_{pq} = \left(\mu_{pq}/\mu_{00}^{(p+q+2)/2}\right)$.

Central moments and scaling-invariant moment representation can be employed to produce a set of invariant moments that are further invariant to symmetric blur and rotation. A set of seven moment invariant functions based on the second- and third-order moments have been first derived by Hu [29]. These functions are invariant to scaling, translation, and rotation. Wong [30] has later proposed a method to generate an infinite sequence of rotation moment invariants and has shown that Hu's invariants are just particular representatives of them. Recently, Flusser and Suk [28] have shown that some odd-order Wong's invariants (or certain simple functions of them) are also blur invariants. Based on this, the set of combined invariants (features that are based on image moments and that are invariant to symmetric blur, scaling, translation, and rotation) used in this work are those introduced in [28] and are given by the following equations:

$$\Phi_1 = (\nu_{30}-3\nu_{12})^2+(3\nu_{21}-\nu_{03})^2 \tag{5}$$

$$\Phi_2 = (\nu_{30}+\nu_{12})^2+(\nu_{21}+\nu_{03})^2 \tag{6}$$

$$\begin{aligned}\Phi_3 = {} & (\nu_{30}-3\nu_{12})(\nu_{30}+\nu_{12})\left((\nu_{30}+\nu_{12})^2-3(\nu_{21}+\nu_{03})^2\right) \\ & +(3\nu_{21}-\nu_{03})(\nu_{21}+\nu_{03})\left(3(\nu_{30}+\nu_{12})^2-(\nu_{21}+\nu_{03})^2\right)\end{aligned} \tag{7}$$

$$\begin{aligned}\Phi_4 = {} & (3\nu_{21}-\nu_{03})(\nu_{30}+\nu_{12})\left((\nu_{30}+\nu_{12})^2-3(\nu_{21}+\nu_{03})^2\right) \\ & -(\nu_{30}-3\nu_{12})(\nu_{21}+\nu_{03})\left(3(\nu_{30}+\nu_{12})^2-(\nu_{21}+\nu_{03})^2\right)\end{aligned} \tag{8}$$

$$\begin{aligned}\Phi_5 = {} & \left[\nu_{50}-10\nu_{32}+5\nu_{14}-10(\nu_{20}\nu_{30}-\nu_{30}\nu_{02}-3\nu_{12}\nu_{20}\right. \\ & \left.+3\nu_{12}\nu_{02}-6\nu_{11}\nu_{21}+2\nu_{11}\nu_{03})\right]^2 \\ & +\left[\nu_{05}-10\nu_{23}+5\nu_{41}-10(\nu_{02}\nu_{03}-\nu_{03}\nu_{20}-3\nu_{21}\nu_{02}\right. \\ & \left.+3\nu_{21}\nu_{20}-6\nu_{11}\nu_{12}+2\nu_{11}\nu_{30})\right].^2\end{aligned} \tag{9}$$

It was shown by Flusser and Suk [28] that these combined invariants are sufficiently robust with respect to noise. The local displacement of every CP in the sensed image can be estimated over a circular neighborhood of each one of these points detected earlier. After that, the correspondence is established by the minimum distance rule with thresholding in the Euclidean space of the invariants. The distance between two different circular templates W_1 and W_2 is defined as

$$d_r(w_1, w_2) = \left\| \vec{C}(r)^{(w_1)} - \vec{C}(r)^{(w_2)} \right\| \tag{10}$$

where $\|\cdot\|$ is the Euclidean norm in $l_2(r)$ space and the vector $\vec{C}(r)$ of combined invariants is defined as

$$\vec{C}(r) = (\Phi_1, \Phi_2, \ldots, \Phi_r) \tag{11}$$

where r is the number of the combined invariants corresponding to the size of $\vec{C}(r)$ (here, $r = 5$). The smaller the distance, the more similar the two regions. In the case of optimal alignment, the distance between the two windows is nil.

2) Template Matching Algorithm: The displacements of CPs are determined by carrying out the following steps.

- Step 1) For every control point p_i, choose a moving circular template W_1 of radius ρ centered at this point in the reference image.
- Step 2) Assuming that misregistration parameters would not exceed an "L" pixel shift for image translation, calculate the combined invariants vectors $\vec{C}(r)^{(W_1)}$ and $\vec{C}(r)^{(W_2)}$ of W_1 and the corresponding template W_2 centered at q_j in the sensed image, respectively.
- Step 3) Calculate the distance d_r between the combined invariants vectors of these two templates in the invariant space, taking into consideration the amount of the maximum translational shift. Save the translational shift giving the minimum distance. To simplify the search process, the preliminary false matches between template pairs are excluded if their distances in the Euclidean space of the invariants are above a certain threshold T_d. At the end, the values of the translational shifts will correspond to the displacements of the selected control points up to integer precision.
- Step 4) The control point $q_i \in Q$ in the sensed image that might correspond to the candidate point $p_i \in P$ in the reference image is determined by the shift position giving the minimum distance.

3) Subpixel Precision: Many applications like change detection, passive navigation, feature location measurements in remote sensing, and image sequence analysis require registration results with an error less than one pixel (subpixel accuracy) [31]. Therefore, it is necessary to provide means to obtain subpixel precision in the displacements computation because the described matching approach only determines the displacements up to integer precision. Since the image pixels constitute the only available information about the represented scene, this inevitably requires some form of interpolation. In order to obtain subpixel accuracy in the displacements computation, several approaches have been proposed, such as analytical match-interpolation methods and image-interpolation methods [19]. In the image interpolation approach, subpixel accuracy can be achieved by translating the mask image by subpixel increments in the local region around the initial best match position [32]. This method is computationally very expensive compared to the analytical match-interpolation methods. An analytical match-interpolation method [19], [33] is used in this paper. In this case, subpixel accuracy is achieved by interpolating in the match measure surface to estimate the position of the peak. Separate horizontal and vertical quadratic interpolation is used to refine the estimates of the two components of each control point p_i. Given the discrete match measure surface $M(u, v)$, corresponding to the previously defined distance d_r between the template in the sensed image at coordinates (u, v) and the one in the reference

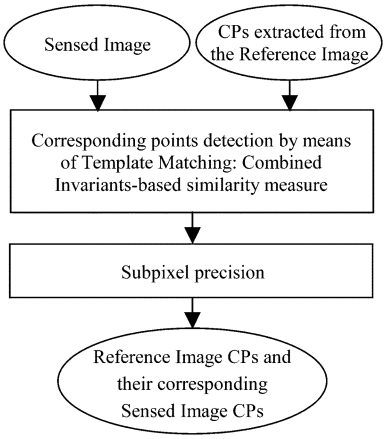

Fig. 4. Block diagram of the CPs displacements computation.

image at the corresponding coordinates (u', v'), and given a best match position (x_0, y_0), then the estimated continuous coordinates (x, y) of the match peak around (x_0, y_0) are calculated as

$$x = x_0 - \frac{1}{2} + \frac{M(x_0, y_0) - M(x_0 - 1, y_0)}{2M(x_0, y_0) - M(x_0 - 1, y_0) - M(x_0 + 1, y_0)}$$
$$y = y_0 - \frac{1}{2} + \frac{M(x_0, y_0) - M(x_0, y_0 - 1)}{2M(x_0, y_0) - M(x_0, y_0 - 1) - M(x_0, y_0 + 1)}. \quad (12)$$

The exact coordinates (x_i, y_i), in the sensed image of each control point p_i, $i = 1, 2, \ldots, n$, constitute the second set of control points $Q = \{q_i\}$ with $q_i = (x_i, y_i)$, $i = 1, 2, \ldots, n$. This template matching method is described in Fig. 4.

C. Image Warping

Given the two sets of corresponding control points, $P = \{p_i\}$ and $Q = \{q_i\}$, the transformation parameters are estimated and the correction is performed by warping the sensed image. Satellite image warping can be performed by applying an affine transform [5], [21]. The affine mapping function is appropriate for data with flat topography. For some data with nonlinear, local geometric distortions (such as hilly areas with terrain changes), more complex transformation functions may be needed to produce better interpolation results. These mapping functions include thin-plate spline interpolation. Thin-plate splines are perhaps the most widely used transformation functions in the registration of images with nonlinear geometric differences. They were first used by Goshtasby [15] in the registration of remote sensing images. This interpolation model plays an essential role to reach subpixel accuracy. Other warping functions such as B-splines have been used to achieve subpixel accuracy [9], [13]. In this paper, sensed image warping has been performed by applying the TPS interpolation function [23] on the two sets of corresponding CPs. The proposed algorithm, using the TPS interpolation, has been designed to be applied on satellite images as well as on low-altitude aerial pictures of rough terrain.

The thin-plate splines are interpolating functions, representing, exactly, the distortion at each CP and defining a minimum-curvature surface between CPs. The TPS function is a flexible transformation that allows rotation, translation, scaling, and skewing. It also allows lines to bend according to the thin-plate spline model. Therefore, a large number of deformations can be characterized by the thin-plate spline model. The thin-plate spline interpolation function can be written as

$$\mathbf{h}(\mathbf{x}) = \mathbf{A}\mathbf{x} + \mathbf{t} + \sum_{i=1}^{n} \mathbf{W_i} K(\|\mathbf{x} - \mathbf{x}_i\|) \quad (13)$$

where $\mathbf{A}$ and $\mathbf{t}$ are the affine transformation parameter matrices, $\mathbf{W}_i$ are the weights of the nonlinear radial interpolation function K, and $\mathbf{x}_i$ are the CPs. The function $K(\lambda)$ is the solution of the biharmonic equation $(\Delta^2 K = 0)$ that satisfies the condition of bending energy minimization, namely $K(\lambda) = \lambda^2 \log(\lambda^2)$.

To solve for the x, y components, the transformation $\mathbf{h}$ is defined from two sets of n corresponding CP pairs as

$$\begin{pmatrix} x' \\ y' \end{pmatrix} = \begin{pmatrix} h_x(x, y) \\ h_y(x, y) \end{pmatrix} = \begin{pmatrix} a_{11} & a_{12} \\ a_{21} & a_{22} \end{pmatrix} \cdot \begin{pmatrix} x \\ y \end{pmatrix} + \begin{pmatrix} t_x \\ t_y \end{pmatrix} + \begin{pmatrix} \sum_{i=1}^{n} W_{xi} K(\|(x, y) - (x_i, y_i)\|) \\ \sum_{i=1}^{n} W_{yi} K(\|(x, y) - (x_i, y_i)\|) \end{pmatrix} \quad (14)$$

where (x', y') and (x, y) are two corresponding CPs in the reference image and the sensed image, respectively.

The warping of the sensed image with respect to the reference image is accomplished by carrying out the following steps.

Step 1) Given the sets P and Q of corresponding coordinates, the estimation of the affine transformation parameters $\mathbf{A}$ and $\mathbf{t}$ is performed by using only the three initial control point pairs having the minimum distance in the Euclidean space of the invariants. These parameters are obtained by solving the following equation in a least square sense:

$$\mathbf{Y} = \mathbf{M}\mathbf{z} \quad (15)$$

where

$$\mathbf{Y} = \begin{bmatrix} x'_1 \\ y'_1 \\ x'_2 \\ y'_2 \\ x'_3 \\ y'_3 \end{bmatrix} \quad \mathbf{M} = \begin{bmatrix} x_1 & y_1 & 0 & 0 & 1 & 0 \\ 0 & 0 & x_1 & y_1 & 0 & 1 \\ x_2 & y_2 & 0 & 0 & 1 & 0 \\ 0 & 0 & x_2 & y_2 & 0 & 1 \\ x_3 & y_3 & 0 & 0 & 1 & 0 \\ 0 & 0 & x_3 & y_3 & 0 & 1 \end{bmatrix}$$

$$\mathbf{z} = \begin{bmatrix} a_{11} \\ a_{12} \\ a_{21} \\ a_{22} \\ t_x \\ t_y \end{bmatrix}.$$

a_{11}, a_{12}, a_{21}, a_{22}, t_x, and t_y are the affine transformation parameters and are found by taking the inverse of the matrix $\mathbf{M}$.

$$\mathbf{z} = \mathbf{M}^{-1}\mathbf{Y} \tag{16}$$

where $\mathbf{M}^{-1}$ is the inverse of $\mathbf{M}$. Based on this transformation, it is possible to map the other control points in the sensed image into the reference image.

Step 2) The invalid control point pairs are removed during this step. The distance between the mapped control point in the sensed image and the actual point in the reference image is computed. This distance is actually the RMSE at this pair of corresponding points. A threshold can be easily set to avoid false matches. The invalid control point pairs can be removed by examining the following condition:

$$\sqrt{(\hat{x}_i - x'_i)^2 + (\hat{y}_i - y'_i)^2} < E_r \tag{17}$$

where (x'_i, y'_i) and $(\hat{x}_i, \hat{y}_i)$ are the coordinates of the control point pairs in the reference image and the affine transformed sensed image, respectively, and $\hat{x}_i = a_{11}x_i + a_{12}y_i + t_x$ and $\hat{y}_i = a_{21}x_i + a_{22}y_i + t_y$. E_r is a preset threshold that is actually the maximum RMSE allowed at the control points for the final image registration. If this condition is satisfied, the pair of points is kept for further processing (i.e., sensed image resampling). If not, this pair of points is removed from the set of corresponding control points. The output from this step is a set of m corresponding control point pairs.

Step 3) The two sets of m corresponding control point pairs are then used to calculate the weights W_{xi} and W_{yi} of the TPS function using the equations

$$\begin{bmatrix} x'_1 - a_{11}x_1 - a_{12}y_1 - t_x \\ x'_2 - a_{11}x_2 - a_{12}y_2 - t_x \\ \vdots \\ x'_m - a_{11}x_m - a_{12}y_m - t_x \end{bmatrix} = \begin{bmatrix} 0 & K(\lambda_{12}) & \dots & K(\lambda_{1m}) \\ K(\lambda_{21}) & 0 & \dots & K(\lambda_{2m}) \\ \vdots & \vdots & & \vdots \\ K(\lambda_{m1}) & K(\lambda_{m2}) & \dots & 0 \end{bmatrix} \begin{bmatrix} W_{x1} \\ W_{x2} \\ \vdots \\ W_{xm} \end{bmatrix} \tag{18}$$

$$\begin{bmatrix} y'_1 - a_{21}x_1 - a_{22}y_1 - t_y \\ y'_2 - a_{21}x_2 - a_{22}y_2 - t_y \\ \vdots \\ y'_m - a_{21}x_m - a_{22}y_m - t_y \end{bmatrix} = \begin{bmatrix} 0 & K(\lambda_{12}) & \dots & K(\lambda_{1m}) \\ K(\lambda_{21}) & 0 & \dots & K(\lambda_{2m}) \\ \vdots & \vdots & & \vdots \\ K(\lambda_{m1}) & K(\lambda_{m2}) & \dots & 0 \end{bmatrix} \begin{bmatrix} W_{y1} \\ W_{y2} \\ \vdots \\ W_{ym} \end{bmatrix} \tag{19}$$

where $\lambda_{i,j} = ||(x_i, y_i) - (x_j, y_j)||$, $1 \le i \le m$, $1 \le j \le m$, and (x_i, y_i) and (x_j, y_j) are the coordinates of the m control points in the sensed image.

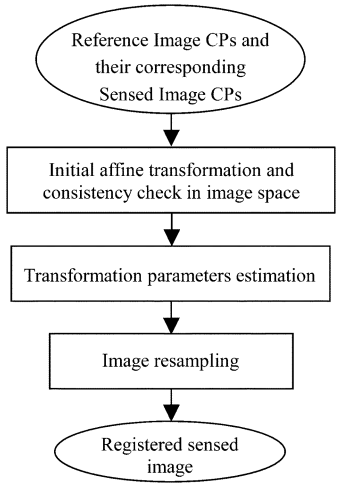

Fig. 5. Schematic diagram for the sensed image warping method.

Step 4) The complete set of parameters, defining the interpolating registration transformation is then used to transform the sensed image values. It should be noted that in order to be able to carry out the warping of the sensed image with respect to the reference image, it is required to have a complete description of the TPS interpolation function (14). That is, this function must be known for every point in the image. So far, only the method for computing the TPS function of a selected set of control points has been described in this paper, under the assumption that the remainder of the field could be obtained by linear interpolation. Detailed algebraic treatment of this TPS-based warping can be found in literature (see [23]).

This warping method is summarized in Fig. 5.

III. Experimental Results and Discussions

To measure the performance of the proposed registration approach, the experimental results were divided into two parts. First, in order to evaluate the accuracy of the registration approach, the proposed method was tested by using a pair of test images: the sensed image being the rotated version of the reference one (see Fig. 6). Second, the proposed method was applied for the registration of multitemporal satellite images from Systeme Pour l'Observbation de la Terre (SPOT) and European Remote Sensing 1 synthetic aperture radar (SAR) sensors. In this latter experiment, two image pairs of the region of Mont Saint-Michel in Normandie (France) were registered separately, one pair of SPOT images and the other one of SAR images acquired at different dates. Subscenes of around 512×512 pixels from the original images were used. The parameters of the Harris detector are set to the standard default values recommended by the authors [26]. The standard deviation of the Gaussian is set to 1 for all examples. During these experiments, the minimum allowed distance between two CPs and the desired number of CPs are set to $d_{\min} = 30$ and $n = 10$. The maximum translational shift used in template matching is set to 100 and the radius ρ of the circular templates is 20. There is no simple

criterion for the template radius ρ. In order to reduce the computation time to a minimum, this template should be as small as possible. However, in principle, the size of the template determines the amount of statistical information that is provided. Small templates will yield unreliable match values. Experiments in this work have indicated that a template of radius size between 10 and 20 pixels yields a good compromise between computational speed and statistical reliability. To identify the most robust matches, the distance threshold in the Euclidean space of the invariants T_d is set to 0.1 and the maximum RMSE (E_r) allowed at the CPs is set to 0.3.

The registration results of this method were compared with those of manual methods. In the existing methods, the root mean square error (RMSE) between the matched CPs provides a measure of registration (20). The RMSE at m matched CPs (in pixels) is defined as in (20), shown at the bottom of the page.

A. Comparison of the Proposed Affine Registration Results With Those of the Manual Registration

For a good evaluation of the performance of the proposed algorithm, distinct corner points were manually selected as CPs on two SPOT images, a reference image and its rotated version as the sensed image (see Fig. 6). The transformation parameters and RMSEs obtained by manual CP selection and registration were compared with those of the proposed automatic CP selection and affine registration with no TPS (see Table I). Hence, the RMSEs in this case have been obtained for both the manual and automatic methods according to (20) using just the affine parameters without the terms related to the TPS function. Ten pairs of CPs are manually selected to register the two images. The number of manually selected CPs and the number of CPs generated by the proposed algorithm are kept the same in order to compare their RMSEs. Thus, to apply the automatic proposed method, the ten selected CPs in the reference image were kept the same as those of the manual method in order to automatically generate the corresponding points on the sensed image. From Table I, it is clear that the differences between the transformation parameters of the manual registration method and that of the proposed one are considerable. The RMSE difference between them is greater than two pixels. The transformation parameters obtained by the proposed registration approach are very close to the optimum values (i.e., the true/known transformation parameters). Clearly the image registration, using the proposed algorithm, results in a lower RMSE, and its accuracy is therefore better than that of the manual one.

B. Registration of Multitemporal SPOT and SAR Images

The results of the application of the proposed registration technique to a pair of SPOT and SAR images acquired at different dates are shown in Figs. 7 and 8. In these figures, four images are chosen for each pair: (a) the reference image, (b) the sensed image, (c) the registered sensed image, and (d) the registration result of the two images after registration. Based on the algorithm parameters set, there are ten CPs in the reference image that were automatically detected by the improved Harris corner detector. The corresponding CPs in the sensed image are computed by means of template matching using the combined invariants-based similarity measure. The coordinates of all CPs determined after application of the image matching step of the algorithm are summarized in Table II.

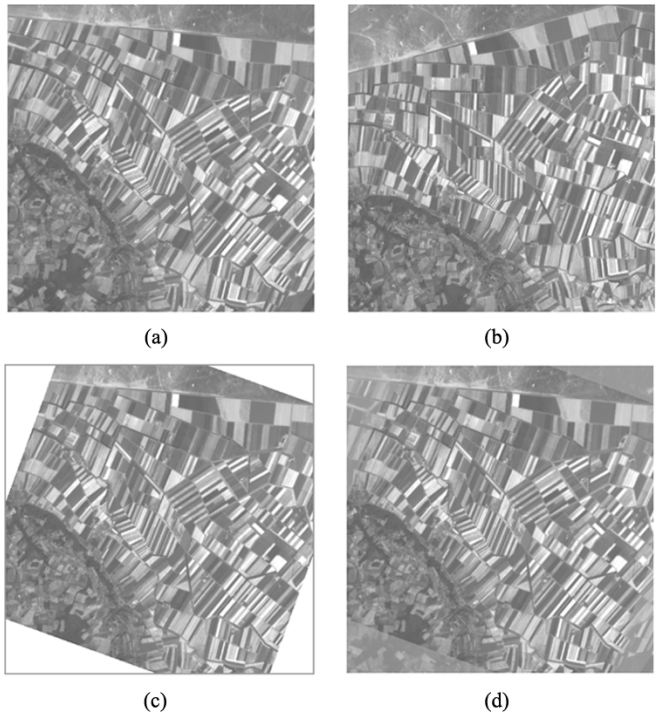

Fig. 6. Registration of a pair of test images. (a) Initial SPOT image. (b) Rotated image by a 10° clockwise rotation of the initial image. The center of rotation is the center of the image. (c) Image (b) after geometric transformation. (d) The registration result using the proposed approach.

TABLE I
COMPARISON OF THE PROPOSED AUTOMATIC REGISTRATION RESULTS WITH THE MANUAL REGISTRATION RESULTS AND WITH GROUND TRUTH

Methods	a_{11}	a_{12}	a_{21}	a_{22}	t_x	t_y	RMSE
Optimal	0.9396	0.3420	-0.3420	0.9396	0.0000	0.0000	0.0000
Manual	0.9450	0.3501	-0.3440	0.9470	0.9503	1.5602	2.8162
Proposed Method	0.9395	0.3422	-0.3419	0.9397	0.0504	3.2e-05	0.0385

Given a number of matched corresponding control points from two images, the affine transformation parameters can be estimated. The registration of images with rotational, translational, scaling, and image-skew differences can be approximated by applying the mapping functions of (14). The

$$\text{RMSE} = \sqrt{\frac{\sum_{i=1}^{m}\left(a_{11}x_i + a_{12}y_i + t_x + \sum_{j=1}^{m} W_{xj}K(\lambda_{ij}) - x_i'\right)^2 + \left(a_{21}x_i + a_{22}y_i + t_y + \sum_{j=1}^{m} W_{yj}K(\lambda_{ij}) - y_i'\right)^2}{m}} \tag{20}$$

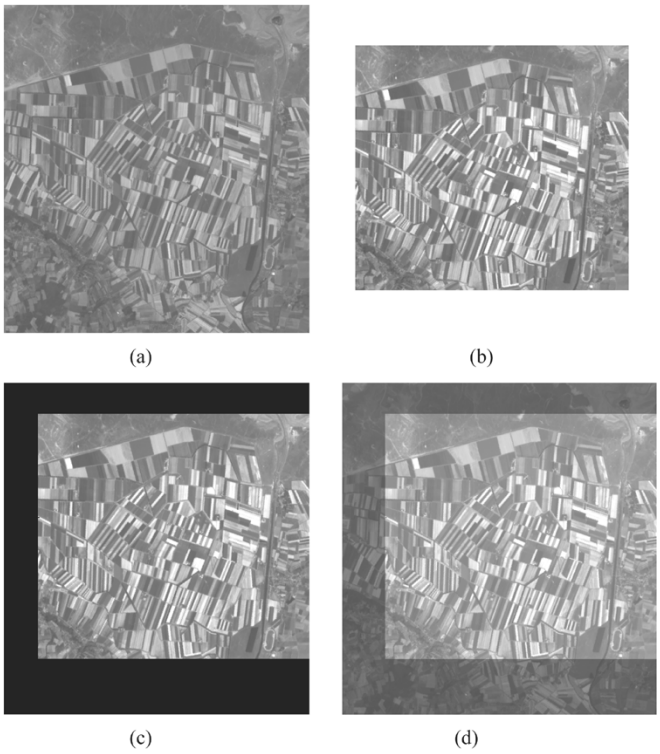

Fig. 7. Registration of SPOT panchromatic images of the region of Mont Saint-Michel in Normandie (France), acquired at different dates. (a) The reference image. (b) The sensed image. (c) The registered sensed image obtained after application of the proposed approach. (d) The registration result.

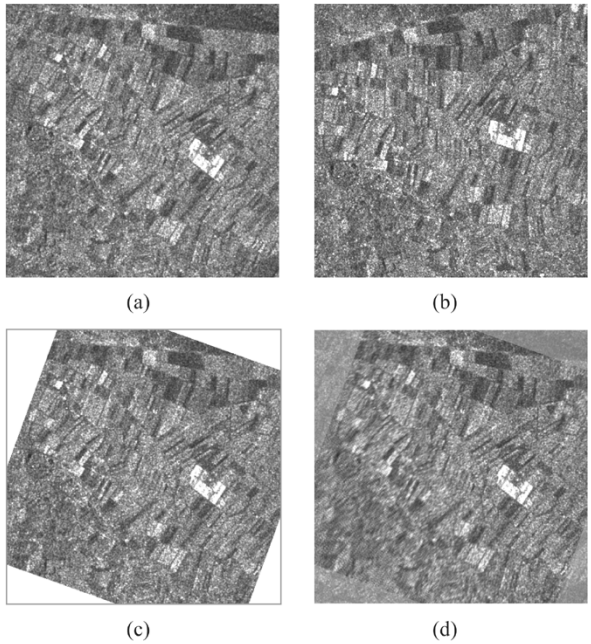

Fig. 8. Registration of SAR images of the region of Mont Saint-Michel in Normandie (France), acquired at different dates. (a) The reference image. (b) The sensed image. (c) The registered sensed image obtained after application of the proposed approach. (d) The registration result.

thin plate-spline transformation function is appropriate for satellite images with nonlinear, local geometric distortions and is needed to produce better interpolation results and to achieve subpixel accuracy. For this type of transformation, the affine transformation parameters and the weights of the nonlinear radial interpolation function are computed in order to resample and transform the sensed image according to the reference image. Since the determination of the affine transformation parameters requires the knowledge of only three CPs, three pairs of CPs with minimum distance were detected and used to estimate these parameters. Based on this affine transformation, the invalid CP pairs (i.e., false matches) are removed if the RMS error (E_r) exceeds a specified threshold as shown in (17). In this case, seven additional matched points were detected in the pair of SPOT and SAR images. An RMSE of less than 0.3 pixels has been obtained for the ten CPs. Knowing the TPS mapping function, the sensed image was transformed and resampled using linear interpolation. The results of the proposed approach are shown in Figs. 7(c) and 8(c).

The registration accuracy of the proposed method was estimated using the RMSE of (20) at every CP, as shown in Table III. RMSE1 denotes the errors after registering two multitemporal SPOT images, while RMSE2 denotes the errors after registering two multitemporal SAR images. The results show that in the proposed automated algorithm, most errors (RMSEs) are less than 0.3 pixels. In this approach, the estimation of the affine transformation parameters is performed by using only the three CPs having the minimum distance among the ten (control points 1, 2, and 3; see Table III). This has the following two advantages.

TABLE II
COORDINATES OF CORRESPONDING CONTROL POINTS IN THE TWO PAIRS OF IMAGES

Control Point	SPOT Images		SAR Images	
	Reference (x, y)	Sensed (x', y')	Reference (x, y)	Sensed (x', y')
1	(450, 453)	(533.99, 513.96)	(285, 48)	(369.98, 75.94)
2	(140, 96)	(223.97, 156.98)	(385, 84)	(452.16, 143.92)
3	(38, 189)	(122.01, 250.02)	(416, 146)	(459.95, 212.90)
4	(37, 324)	(120.88, 384.98)	(398, 274)	(399.10, 327.12)
5	(113, 439)	(197.08, 499.88)	(364, 417)	(316.88, 451.07)
6	(206, 467)	(290.07, 527.77)	(236, 434)	(188.99, 422.96)
7	(378, 437)	(461.97, 498.11)	(73, 302)	(81.12, 243.03)
8	(506, 358)	(589.88, 419.02)	(38, 167)	(94.98, 103.97)
9	(475, 249)	(559.01, 309.97)	(116, 134)	(180.12, 99.07)
10	(498, 149)	(582.10, 210.01)	(277, 147)	(328.09, 166.10)

TABLE III
ROOT MEAN SQUARE ERRORS AT THE CONTROL POINTS (IN PIXELS)

CP	1	2	3	4	5	6	7	8	9	10	Total CPs RMSE
RMSE1	0.0252	0.0061	0.0067	0.1698	0.1717	0.2679	0.1173	0.0977	0.0806	0.2119	0.1433
RMSE2	0.0087	0.0122	0.0118	0.2272	0.2253	0.2208	0.2559	0.1888	0.0705	0.0288	0.1607

1) The computation time is reduced with respect to processing all the detected control points.
2) The use of only three control points with minimum distance enhance more the accuracy of the affine transformation parameters estimation and thus the effectiveness of the registration than that using the entire ten points some of them having no minimum distance. The total control points RMSE in this case is around 0.1 pixels, which is a very high accuracy.

In general, image registration, using the proposed algorithm, results in a lower RMSE.

The proposed algorithm has several user-defined parameters, namely the number n of CPs, the minimum allowed distance

$d_{\min}$ between the points, the radius ρ of the circular template, and the maximum translational shift L used for template matching. Increasing the parameters ρ, L, and n slows down the registration but may enhance the accuracy and robustness. When the geometric deformations between the images are large and fast registration is needed, applying a coarse rigid preregistration before extracting the corresponding points is recommended. This will reduce the required maximum translational shift used in template matching and, consequently, increase the speed of registration. The choice of the parameters is influenced by the type of the scene. The proposed algorithm was successfully tested on one scene. In the case of highly textured scenes where features may not be reliably observed, a large number of CPs can be selected corresponding to reference image corners or highly textured patches. Since the estimation of the transformation parameters is sensitive to location errors when the features are close to each other, it is convenient to spread out the detected CPs by setting the minimum allowed distance parameter $d_{\min}$ between two CPs high. The template matching stage of the algorithm [i.e., Steps 1)–4)] of Section II-B2 may generate a false match, for example, due to repetitive texture patterns. In this case, the use of large templates for feature matching allows for a reliable correspondence between the images. This algorithm is quite robust and reliable as long as corresponding distinctive points are available in the images. The registration scheme would fail if the input images did not contain distinctive features, e.g., the case of mountainous scenes without any distinctive features. However, in such situation, almost every feature-based matching procedure will fail.

IV. Conclusion

In this paper, a new approach to the registration of remotely sensed data is proposed and tested on one scene. In this approach, a new strategy was developed in which a global transformation function is estimated by only three control points with the best match. Therefore, the registration accuracy of the proposed method is much higher than that of traditional methods. The method involves the extraction of a set of CPs where misalignment between images can be expected to appear. These CPs are obtained by thresholding the gradient magnitude of the reference image and by applying the improved version of the well-known Harris corner detector. The corresponding set of CPs in the sensed image is determined by means of template matching, using the combined invariants-based similarity measure. Of all similarity measures developed so far, the combined invariants-based measure was demonstrated to satisfy the three constraints that have been emphasized in the introduction of this paper and therefore to be the most adequate measure for registration of remotely sensed images. After establishing the correspondence between small templates in the two images (reference and sensed), the central points of the corresponding templates in the sensed image are used as the corresponding set of CPs. The parameters of the affine transformation are computed by using only three pairs of CPs with the best match (minimum distance in the Euclidean space). The final correction is accomplished by warping the sensed image with respect to the reference image by using the thin-plate spline-based interpolation. The performance of the proposed registration algorithm has been demonstrated by registering two multitemporal SPOT images and two multitemporal SAR images taken in different dates from one scene. In the experiments, a registration accuracy of less than 0.3 pixels has been achieved at each individual CP and an RMSE of less than 0.2 pixels has been obtained for the ten CPs. Moreover, the proposed registration has a better performance than the manual one, with an improvement in the registration accuracy of more than two pixels. This automatic algorithm is really fast and yields accurate global and local registrations. The approach is also robust, since it overcomes the difficulties of CP correspondence caused by the problem of feature inconsistency. The proposed registration technique may be applied to other satellite data as well as to airborne scanner data. In future work, the algorithm will be tested on other types of datasets, and its performance will be compared to other registration techniques.

References

[1] X. Dai and S. Khorram, "The effects of image misregistration on the accuracy of remotely sensed change detection," *IEEE Trans. Geosci. Remote Sens.*, vol. 36, no. 5, pp. 1566–1577, Sep. 1998.

[2] ——, "A hierarchical methodology framework for multisource data fusion in vegetation classification," *Int. J. Remote Sens.*, vol. 19, no. 18, pp. 3697–3701, Dec. 1998.

[3] L. G. Brown, "A survey of image registration techniques," *ACM Comput. Surv.*, vol. 24, no. 4, pp. 325–376, Dec. 1992.

[4] B. Zitova and J. Flusser, "Image registration methods: A survey," *Image Vis. Comput.*, vol. 21, no. 11, pp. 977–1000, Apr. 2003.

[5] H. Li, B. S. Manjunath, and S. K. Mitra, "A contour-based approach to multisensor image registration," *IEEE Trans. Image Process.*, vol. 4, no. 3, pp. 320–334, Mar. 1995.

[6] Q. Zheng and R. Chellappa, "A computational vision approach to image registration," *IEEE Trans. Image Process.*, vol. 2, no. 7, pp. 311–326, Jul. 1993.

[7] F. Maes, A. Collignon, D. Vandermeulen, G. Marchal, and P. Suetens, "Multimodality image registration by maximization of mutual information," *IEEE Trans. Med. Imag.*, vol. 16, no. 2, pp. 187–198, Apr. 1997.

[8] W. M. Wells, III, P. Viola, H. Atsumi, S. Nakajima, and R. Kikinis, "Multi-modal volume registration by maximization of mutual information," *Med. Imag. Anal.*, vol. 1, pp. 35–51, 1996.

[9] P. Thevenaz and M. Unser, "Optimization of mutual information for multiresolution image registration," *IEEE Trans. Image Process.*, vol. 9, no. 12, pp. 2083–2099, Dec. 2000.

[10] J. Le Moigne, W. J. Campbell, and R. F. Cromp, "An automated parallel image registration technique based on the correlation of wavelet features," *IEEE Trans. Geosci. Remote Sens.*, vol. 40, no. 8, pp. 1849–1864, Aug. 2002.

[11] J. Le Moigne and I. Zavorin, "Use of wavelets for image registration," in *Proc. SPIE Aerosense 2000, Wavelet Applications VII*, Orlando, FL, Apr. 24–28, 2000.

[12] K. Johnson, A. Cole-Rhodes, I. Zavorin, and J. Le Moigne, "Mutual information as a similarity measure for remote sensing image registration," in *Proc. SPIE Aerosense 2001, Geo-Spatial Image and Data Exploitation II*, vol. 4383, Orlando, FL, Apr. 2001, pp. 51–61.

[13] A. A. Cole-Rhodes, K. L. Johnson, J. Le Moigne, and I. Zavorin, "Multiresolution registration of remote sensing imagery by optimization of mutual information using a stochastic gradient," *IEEE Trans. Image Process.*, vol. 12, pp. 1495–1511, Dec. 2003.

[14] J. Flusser and T. Suk, "A moment-based approach to registration of images with affine geometric distortion," *IEEE Trans. Geosci. Remote Sens.*, vol. 32, no. 3, pp. 382–387, Mar. 1994.

[15] A. Goshtasby, "Registration of images with geometric distortions," *IEEE Trans. Geosci. Remote Sens.*, vol. 26, no. 1, pp. 60–64, Jan. 1988.

[16] J. Ton and A. K. Jain, "Registering landsat images by point matching," *IEEE Trans. Geosci. Remote Sens.*, vol. 27, no. 5, pp. 642–651, Sep. 1989.

[17] B. S. Reddy and B. N. Chatterji, "An FFT-based technique for translation, rotation, and scale-invariant image registration," *IEEE Trans. Image Process.*, vol. 5, no. 8, pp. 1266–1271, Aug. 1996.
[18] J. P. Djamdji, A. Bijaoui, and R. Maniere, "Geometrical registration of images: The multiresolution approach," *Photogramm. Eng. Remote Sens.*, vol. 59, no. 5, pp. 645–653, May 1993.
[19] Y. Bentoutou, N. Taleb, M. Chikr El Mezouar, M. Taleb, and L. Jetto, "An invariant approach for image registration in digital subtraction angiography," *Pattern Recognit.*, vol. 35, no. 12, pp. 2853–2865, Dec. 2002.
[20] E. J. M. Rignot, R. Kowk, J. C. Curlander, and S. S. Pang, "Automated multisensor registration: Requirements and techniques," *Photogramm. Eng. Remote Sens.*, vol. 57, pp. 1029–1038, Aug. 1991.
[21] X. Dai and S. Khorram, "A feature-based image registration algorithm using improved chain-code representation combined with invariant moments," *IEEE Trans. Geosci. Remote Sens.*, vol. 37, no. 5, pp. 2351–2362, Sep. 1999.
[22] P. Dare and I. Dowman, "An improved model for automatic feature-based registration of SAR and SPOT images," *ISPRS J. Photogramm. Remote Sens.*, vol. 56, no. 1, pp. 13–28, Jun. 2001.
[23] F. L. Bookstein, "Principal warps: Thin-plate splines and the decomposition of deformations," *IEEE Trans. Pattern Anal. Mach. Intell.*, vol. 11, no. 6, pp. 567–585, Jun. 1989.
[24] C. Schmid and R. Mohr, "Local gray value invariants for image retrieval," *IEEE Trans. Pattern Anal. Mach. Intell.*, vol. 19, no. 5, pp. 530–535, May 1997.
[25] J. F. A. Canny, "Computational approach to edge detection," *IEEE Trans. Pattern Anal. Mach. Intell.*, vol. PAMI-8, no. 6, pp. 679–698, Nov. 1986.
[26] C. Schmid, R. Mohr, and C. Bauckhage, "Evaluation of interest point detectors," *Int. J. Comput. Vis.*, vol. 37, no. 2, pp. 151–172, Jun. 2000.
[27] C. Harris and M. Stephens, "A combined corner and edge detector," in *Proc. 4th Alvey Vision Conf.*, Manchester, U.K., 1988, pp. 147–151.
[28] J. Flusser and T. Suk, "Degraded image analysis: An invariant approach," *IEEE Trans. Pattern Anal. Mach. Intell.*, vol. 20, no. 6, pp. 590–603, Jun. 1998.
[29] M. K. Hu, "Visual pattern recognition by moment invariants," *IRE Trans. Inf. Theory*, vol. 8, pp. 179–187, 1962.
[30] W. H. Wong, W. C. Siu, and K. M. Lam, "Generation of moment invariants and their uses for character recognition," *Pattern Recognit. Lett.*, vol. 16, no. 2, pp. 115–123, Feb. 1995.
[31] Q. Tian and M. N. Huhns, "Algorithms for subpixel registration," *Comput. Vis. Graph. Image Process.*, vol. 35, no. 2, pp. 220–223, Aug. 1986.
[32] L. Van Tran and J. Sklansky, "Flexible mask subtraction for digital angiography," *IEEE Trans. Med. Imag.*, vol. 11, no. 3, pp. 407–415, Sep. 1992.
[33] G. S. Cox and G. de Jager, "Automatic registration of temporal image pairs for digital subtraction angiography in medical imaging," in *Proc. SPIE Image Processing*, vol. 2167, Bellingham, WA, Feb. 1994, pp. 188–199.

Youcef Bentoutou received the Eng., Magister, and Doctorate degrees in electrical engineering from the University of Djilali Liabes, Sidi Bel Abbes, Algeria, in 1997, 2000, and 2004 respectively.

Since March 2002, he has been working as a research team leader at the National Center for Space Techniques, Arzew, Algeria. He is also an Associate Researcher in the Communication Networks, Architecture, and Multimedia Laboratory, University of Sidi Bel Abbes. From November 2000 to March 2002, he has been in training at the Surrey Space Centre, University of Surrey. His principal research interests are in the fields of digital signal and image processing, medical and satellite imaging, and onboard data handling. His current work includes the development of image registration methods and the implementation of these methods on field-programmable gate arrays for application to satellite onboard data processing.

Nasreddine Taleb received the M.Sc. degree in computer engineering from Boston University, Boston, MA, the E.E. degree from Northeastern University, Boston, and Doctorat d'Etat degree in electrical engineering from the University of Sidi Bel Abbes, Sidi Bel Abbes, Algeria, in 1985, 1989, and 1999, respectively.

He is currently a Professor in the Department of Electronic Engineering, University of Sidi Bel Abbes, where he has been teaching since 1990. He is also a Senior Research Scientist in the Communication Networks, Architecture, and Multimedia Laboratory at the University of Sidi Bel Abbes. His principal research interests are in the fields of digital signal and image processing, medical imaging, and advanced architectures for implementation of DSP/DIP applications.

Dr. Taleb is a member of the IEEE Signal Processing Society.

Kidiyo Kpalma received the Ph.D. degree in image processing from the National Institute for Applied Sciences of Rennes (INSA), Rennes, France.

He is currently an Assistant Professor in the Department of Electronic and Computer Engineering at INSA. As a member of the Image and Remote Sensing group of the Institute of Electronics and Telecommunications of Rennes (IETR), a research unit linked to the French National Center for Scientific Research, his research interests are in the fields of image analysis, pattern recognition, image fusion, and remote sensing.

Joseph Ronsin is currently a Professor in the Department of Electronic and Computer Engineering, Institut National des Sciences Appliquées de Rennes (INSA), Rennes, France. He is the Co-Responsible of the Image and Remote Sensing research group of the Institut d'Electronique et Télécommunications de Rennes, a research unit linked to the Centre National de la Recherche Scientifique. The INSA Image and Remote Sensing group focuses its research activities on representation and compression of video frames and sequences, analysis and interpretation of remote sensing images, and prototyping on parallel and mixed architectures. He has also been responsible for several industrial grants from public and private laboratories.